Strain intermittency due to avalanches in ferroelastic and porous materials

IOP Publishing Journal of Physics: Condensed Matter
J. Phys.: Condens. Matter **29** (2017) 224002 (7pp) https://doi.org/10.1088/1361-648X/aa6bd2

Strain intermittency due to avalanches in ferroelastic and porous materials

V Soprunyuk[1], S Puchberger[1], A Tröster[2], E Vives[3], E K H Salje[4] and W Schranz[1]

[1] Faculty of Physics, University of Vienna, Boltzmanngasse 5, 1090 Wien, Austria
[2] Institute of Material Chemistry, Vienna University of Technology, Getreidemarkt 9, 1090 Wien, Austria
[3] Departament de Física de la Matéria Condensada, Facultat de Física, Universitat de Barcelona, Martí i Franqués 1, 08028 Barcelona, Catalonia, Spain
[4] Department of Earth Sciences, University of Cambridge, Downing Street CB2 3EQ, Cambridge, United Kingdom

E-mail: wilfried.schranz@univie.ac.at

Received 20 February 2017, revised 5 April 2017
Accepted for publication 6 April 2017
Published 3 May 2017

Abstract

The avalanche statistics in porous materials and ferroelastic domain wall systems has been studied for slowly increasing compressive uniaxial stress with stress rates between 0.2 and 17 kPa s^{-1}. Velocity peaks $v_m = dh/dt$ are calculated from the measured strain drops and used to determine the corresponding Energy distributions $N(E \equiv v_m^2)$. Power law distributions $N(v_m^2) \propto (v_m^2)^{-\varepsilon}$ have been obtained over 4–6 decades. For most of the porous materials and domain wall systems an exponent $\varepsilon = 1.5 \pm 0.1$ was obtained in good agreement with mean-field theory of the interface pinning transition. For charcoal, shale and calcareous schist we found significant deviations of the exponents from mean-field values in agreement with recent acoustic emission experiments.

Keywords: avalanches, pinning, domain walls

(Some figures may appear in colour only in the online journal)

1. Introduction

Avalanches occur in a variety of dynamical systems. They can be induced by slowly increasing external stress e.g. in porous materials [1–3], metals [4–6] or wood [7] as well as in ferromagnetic materials [8, 9] responding to an external magnetic field. Avalanches in disordered ferromagnets manifest themselves as 'Barkhausen jumps' [9, 10] in the hysteresis curve, also known as 'Barkhausen noise'. Sethna *et al* [11] introduced the more general term 'crackling noise' for any signal that some disordered systems produce as a response to an external driving field smoothly changing in time.

In the past years systems showing crackling behaviour have been studied intensely. Despite the steady increase in the external field, crackling signals (jerks) are usually very irregular with different sizes and durations, separated by quiescence intervals. Tiny events occur very frequently, while large events are rare. The probability distributions of individual events with magnitude w, e.g. jerk energies, sizes or durations and waiting times, typically follow power laws $P(w) \propto w^{-\varepsilon}$ that span over many orders of magnitudes [11, 12] with no characteristic size and time scales. This indicates that the crackling behaviour is independent of microscopic details of a system and only depends on general properties, e.g. symmetries or dimensions [12]. Indeed, in a recent work [13] such universal character of quake statistics was shown to be valid for a wide range of materials (rocks, bulk metallic glasses, granular materials) over 12 decades in length scale.

Some time ago it was already stated that there are profound analogies between fracture experiments and earthquakes, but only few attempts were made to characterize such similarities. Recently Baró *et al* [1] studied the acoustic emission events produced during the compression of mesoporous silica (Vycor) obtaining good fulfilment of some fundamental power laws of statistical seismology. Uhl *et al* [13] also found the same scaling behaviour of compressed nanocrystals and earthquakes, and explained this impressing agreement across

scales by a mean field model for avalanches of slipping randomly distributed weak spots. In this model each weak spot fails, when the local stress (as a result of the applied external stress) is larger than the local failure threshold stress, which has a certain spatial distribution. This local failure is accompanied by a local slip whose released stress will be equally redistributed to the other weak spots in the system. This stress redistribution may trigger slip avalanches which can be measured either by a serration in the stress-strain curve or as acoustic emission.

Another class of models which is also frequently used to describe avalanches in a variety of dynamical systems is based on the depinning transition of a slowly driven elastic interface in systems with quenched disorder [14, 15]. As the driving field is slowly increased to a critical value, the elastic interface undergoes a transition from a pinned state to a moving regime. Near this pinning-depinning transition, the motion of the interface proceeds in avalanches with scale-invariant statistics. A perfect system for the study of elastic interfaces in random potentials are domain walls in ferroelastic crystals. Up to now most experiments on ferroelastic domain walls concentrated on its smooth wall propagation and not many data on their intermittent behaviour exist. In a recent experiment Harrison *et al* [16, 17] demonstrated the existence of jerky avalanches for the movement of needle shaped elastic domain walls in the perovskite $LaAlO_3$. From measurements of the movement of a single needle tip under week external stress, they found discrete jumps of the needle tip position $x(t)$ due to pinning/depinning of the needle tip to defects. By calculating the corresponding tip velocities $v = \mathrm{d}x/\mathrm{d}t$ and relating their square values to the dissipated energy $E \propto (\mathrm{d}x/\mathrm{d}t)^2$ they found a power law distribution $N(E) \propto E^{-\varepsilon}$ with $\varepsilon = 1.8 \pm 0.2$.

In the present study we investigate crackling noise during uniaxial compression to compare the avalanche statistics of ferroelastic and porous materials. Many of the previous measurements about the microstrucural evolution leading to avalanches were performed using acoustic emission (AE) [1, 2, 18–21]. This technique is highly sensitive and able to provide information about the statistical characteristics of event energies, their duration and waiting times between events. However, the method has some drawbacks if the samples are small. In the present work we use strain drop measurements to compare systems with different microstructures that show sharp, intermittent responses under uniaxial compression. The elementary processes leading to crackling noise in these systems are rather different. In porous silica avalanches result from nanometre size pores and cavities that are collapsing, whereas in ferroelastics they result from the propagation of domain wall segments. Each of such a nano- or microstructural movement triggers others leading to power laws in charactersistic distributions. It turns out that the power law exponent values obtained from our strain drop measurements follow the same tendencies across different materials as the corresponding power law exponents from acoustic emission (AE).

Sections 2 and 3 describe the experimental technique and sample properties. Results are presented in section 4. Section 5 concludes the paper with a short discussion.

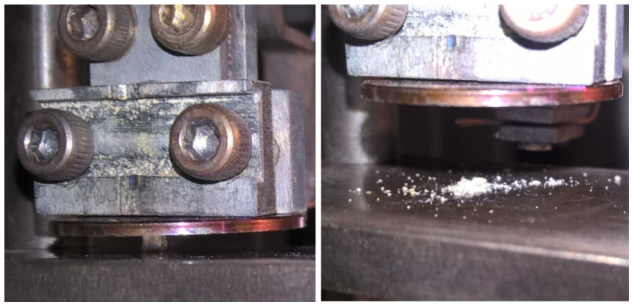

Figure 1. Sample of calcareous schist before and after the compression experiment.

2. Experimental technique

The experimental technique employed in the present study involves the measurement of strain drops at a slowly increasing external stress. A Dynamical Mechanical analyzer (Diamond DMA, Perkin Elmer) offers an adequately low stress rate ($\approx$ 3–120 mN min^{-1}) for inducing intermittent height drops of various millimetre-sized samples during compression experiments. The DMA also measures the response of the sample, in this case the sample height evolution $h(t)$ with time. Figure 1 shows e.g. a calcareous schist sample before and after the compression experiment, yielding complete damage. From the jerky changes of the sample height $h(t)$ we calculate the squared temporal derivatives $v(t)^2 = (\mathrm{d}h/\mathrm{d}t)^2$ and determine the distribution of squared maximal drop velocities $N(v_m^2)$, as shown in [3]. In this way we relate the statistical characteristics of height drops $\Delta h(t)$ to the energy distribution $N(E \equiv v_m^2) \propto (v_m^2)^{-\varepsilon}$ of jerks.

This technique offers some advantages over AE when it comes to micron-scale samples and measurements under different ambient conditions, e.g. different temperatures. With our DMA (Diamond DMA, Perkin Elmer) a temperature range between -180 °C and $+600$ °C can be used. The force can be applied up to 10 N with an accuracy of 0.002 N and the resolution of the sample height is about 10 nm. Unfortunately, the time resolution is limited to 1 s. Additionally, it is also possible to measure the Young's modulus and loss ($\tan\delta$) as function of frequency, temperature and/or stress without changing the measurement geometries.

3. Sample properties

Table 1 lists the different samples, their geomtries and stress rates which were used for uniaxial compression measurements. The first type of materials contains the ferroelastics $LaAlO_3$ and $PbZrO_3$. Vycor and Gelsil are both porous SiO_2-based materials with nanometre pore sizes. The last group consists of various kinds of rocks and charcoal.

$LaAlO_3$ and $PbZrO_3$ are perovskites with ferroelastic properties at room temperature. Lanthanum aluminate undergoes an improper ferroelastic phase transition at 550 °C from cubic $Pm\bar{3}m$ to rhombohedral $R\bar{3}c$ phase [22]. Lead Zirconate exhibits a phase transition [23–25] from a paraelectric phase with cubic symmetry $Pm\bar{3}m$ ($Z = 1$) to an antiferroelectric orthorhombic phase $Pbam$ ($Z = 8$) at $T_c \approx 503$–510 K,

Table 1. Characteristics of the studied samples: initial sample height h_0, cross-section A and compression stress rate $d\sigma/dt$.

Sample	h_0 (mm)	A (mm^2)	$d\sigma/dt$ (kPa s^{-1})
$LaAlO_3$	2.88 ± 0.01	0.94 ± 0.02	0.25 ± 0.01
$PbZrO_3$	1.58 ± 0.01	0.41 ± 0.03	0.61 ± 0.05
Vycor	1.00 ± 0.01	0.25 ± 0.04	6.70 ± 0.16
Gelsil	1.70 ± 0.01	1.00 ± 0.04	0.67 ± 0.01
Shale	0.84 ± 0.01	0.12 ± 0.03	17.00 ± 0.52
Calcareous-Schist	2.13 ± 0.01	2.70 ± 0.02	0.74 ± 0.01
Yellow Sandstone	2.35 ± 0.01	1.43 ± 0.04	0.70 ± 0.01
Charcoal (beech)	2.00 ± 0.01	1.43 ± 0.02	0.70 ± 0.01

depending on crystal quality. The temperature and frequency dependences of domain wall motion of $LaAlO_3$ [26] and $PbZrO_3$ [27] have been studied in very detail by DMA measurements of the complex Young's moduli. In both crystals the domain wall movement is already frozen at room temperature. It means that even at lowest measurement frequencies (0.1 Hz) the domain wall motion cannot follow the externally applied dynamic stress (i.e. $\omega\tau_{DW} > 1$), whereas a crossover to $\omega\tau_{DW} < 1$ occurs at elevated temperature. $LaAlO_3$ and $PbZrO_3$ have been characterized in very detail by XRD rocking curves [26, 22] and TEM [28], respectively. The domain wall thickness was determined by high resolution x-ray diffraction [29] for $LaAlO_3$ (to be of the order of 2 nm) and by electron microscopy [28] for $PbZrO_3$ (revealing a wall thickness of the order of unit cell dimensions).

Vycor and Gelsil are mesoporous silica glasses with different pore sizes. Vycor originates from spinodal decomposition, resulting in a skeleton of nearly pure SiO_2 containing a network of interconnected nm-sized pores of narrow pore size distribution, random in length and direction [30]. Gelsil monoliths are produced in a sol-gel process by hydrolization of silica containing precursors liquids, followed by condensation and heat treatment. Silica molecules condensate to spheres on stochastic sites within the hydrolized silica precursor. Subsequent gelation leads to a network-like arrangement of spheres. After heat treatment the dried and consolidated end product can be approximated as an assembly of stochastically arranged and monodisperse pure silica spheres [31]. These spheres are touching and penetrating each other and the voids between them consitute a random network of inter-connected corridors and pockets. Our Vycor sample has an approximate pore size of 7.5 nm and Gelsil approximately 2.6 nm. Table 2 shows characteristic parameters of porous samples. Both, Vycor and Gelsils are commercial samples and the microstructures of Vycor [30] and Gelsil [32] have been studied thoroughly using transmission electron microscopy.

Shale and calcareous schist are different kinds of rocks. Shale is a laminated, fine-grained and clastic sedimentary rock, composed of tiny fragements of diverse minerals, including quartz and calcite [33]. Recent AE measurements of Baró *et al* [34] revealed that shale exhibits avalanches of stress release under compression. Their results showed that the event energies follow power law statistics quite similar to Vycor [1] but with significantly higher exponent value $\varepsilon_{AE} = 1.73 \pm 0.03$–$1.97 \pm 0.16$ compared with $\varepsilon_{AE} = 1.40 \pm 0.05$. Additionally, they report that

Table 2. Characteristic parameters [30, 35, 36] of porous silica samples.

Properties	Vycor	Gelsil
Pore size (nm)	10.0 ± 0.5	2.6 ± 1
Porosity Φ	0.4	0.36
Pore volume V_{pore} (cm^3 g^{-1})	0.224	0.4

events in shales are uncorrelated and do not follow Omori aftershock behaviour.

Schist is a metamorphic rock which has a foliated or plated structure. The schist used in our measurements is a calcareous shale from a region at the mountain Großglockner, Austria (Gamsgrube).

Yellow sandstone consists of quartz ($\approx$79%), feldspar ($\approx$5%) and clay ($\approx$11%) with an average pore diameter $<$0.1 mm which is four orders of magnitude larger than in synthetic Gelsil and Vycor [2]. AE measurements of yellow sandstone revealed that the energy distribution follows a power law with exponent $\varepsilon_{AE} = 1.49 \pm 0.05$ [2].

Commercial charcoal made of beech wood was used for the experiments.

4. Results

Measuring avalanche statistics is demanding because large data sets are needed for any reliable statistical analysis. A reasonable avalanche analysis requires the observation of at least 1000 jerks. In order to obtain such a large data set we performed cycle measurements with several stress cycles in cases where a a single stress ramp from 0.001–10 N has not delivered enough signals. Stress cycling also increases the probability to achieve macroscopic collapse of the sample.

Figure 2 (left) shows a typical compression experiment of $LaAlO_3$ with one stress cycle. The green line displays the evolution of the sample height $h(t)$ showing rather irregular height drops. From these jumps the blue signal is derived as $v_m^2 = (dh/dt)^2_{max}$. Not all jerks are manifestations of avalanches, they can also be produced by the measuring device or sample vibrations. Therefore, such artefacts have to be eliminated before avalanche statistics based on a jerk spectrum can be discussed. In our measurements usually all jerks with squared velocities $v_m^2 < 10$ nm^2 s^{-2} do not contribute to the power law behaviour. An autocorrelation of the jerk spectrum revealed that the data show a time correlation, however the jerks < 10 nm^2 s^{-2} behave like white noise. This value represents a meaningful threshold since it corresponds to the resolution of the DMA apparatus (i.e. $\approx$10 nm).

Before the jerks are analysed further, we exclude positive jumps (backjumps) whose origin is not yet clear. The jerk data (squared negative jumps only) are then logarithmically binned resulting in a histogram. In contrast to linear binning, logarithmic binning reduces the number of zeros and low count bins at larger values of v_m^2. The histogram bin entries have however to be redefined to correct the effect of logarithmic binning in order to construct a diagram of $N(v_m^2)$. Fitting a

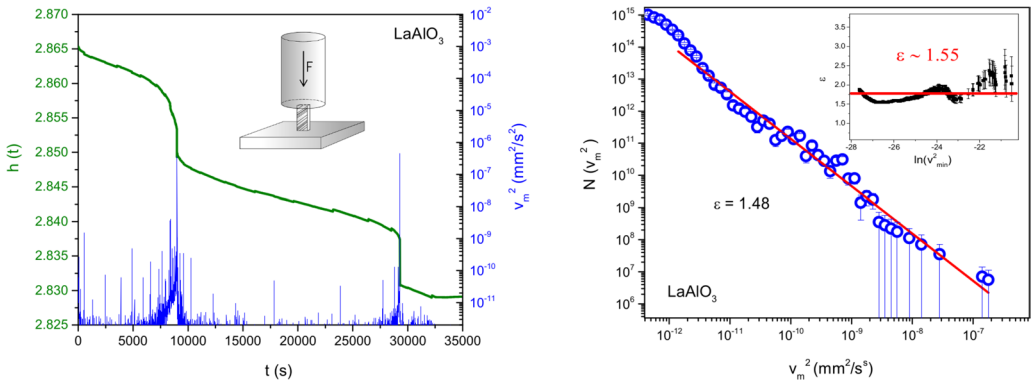

Figure 2. Left: compression experiment of $LaAlO_3$ at room temperature. The green line displays the measured sample height $h(t)$. The applied force is increased at the rate 15 mN min^{-1} from 0.01–9 N. Blue lines show the squared drop velocity maxima $v_m^2 = (dh/dt)^2_{max}$. The inset shows a sketch of the geometrical situation of the compression experiment. Right: log–log plot of the distribution $N(v_m^2)$ of maximum drop velocities squared. The red line displays a power law with exponent $\varepsilon = 1.48 \pm 0.06$. The inset shows the corresponding maximum likelihood plot revealing a plateau at an exponent value of about $\hat{\varepsilon} = 1.55 \pm 0.10$

Table 3. Total number N of v_m^2-peaks used for calculation of the power law distribution, $\hat{\varepsilon}$-exponents which correspond to the approximately constant plateaus obtained from MLE and ε exponent values from fitting of the power law distributions. ε_{AE} and p_{AE} are power law exponents determined from acoustic emission. − means that the corresponding power law exponent was not yet determined.

Sample	N	$\hat{\varepsilon}$	ε	ε_{AE}
$LaAlO_3$	1818	1.55 ± 0.10	1.48 ± 0.06	—
$PbZrO_3$	1151	1.50 ± 0.10	1.47 ± 0.06	—
Vycor	5060	1.70 ± 0.10	1.50 ± 0.05	1.40 ± 0.05 [1]
Gelsil	2850	1.65 ± 0.05	1.55 ± 0.05	1.37 ± 0.03 [2]
Shale	5551	1.70 ± 0.05	1.66 ± 0.03	$1.7 - 1.9$ [34]
Calcareous schist	19095	1.66 ± 0.12	1.66 ± 0.03	—
Charcoal	2339	1.40 ± 0.05	1.33 ± 0.03	1.3 [40]
YSandstone	6581	1.51 ± 0.06	1.48 ± 0.04	1.49 ± 0.05 [2]

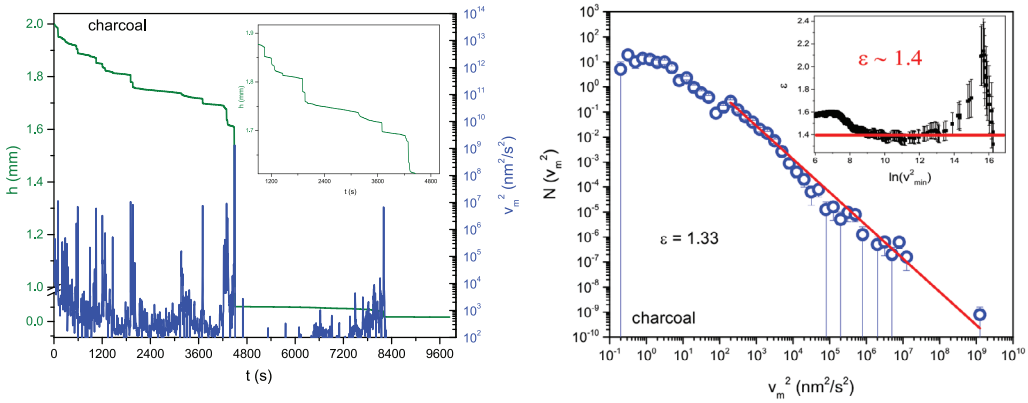

Figure 3. Left: compression experiment of charcoal at room temperature. The green line displays the measured sample height h(t). The applied force is increased at the rate 60 mN min^{-1} from 0.01–10 N. Blue lines show the squared drop velocity maxima $v_m^2 = (dh/dt)^2_{max}$. Inset shows a magnification of h(t). Right: corresponding log–log plot of the distribution $N(v_m^2)$ of maximum drop velocities squared. The red line displays a power law with exponent $\varepsilon = 1.33 \pm 0.03$. The inset shows the corresponding maximum likelihood plot revealing a plateau at an exponent value of about $\hat{\varepsilon} = 1.40 \pm 0.05$

linear slope to the log–log plot of $N(v_m^2)$ yields the exponent value ε of the maximum drop velocities squared distribution. However, binning of the data bears some pitfalls (detailed description in [3]), therefore we complement the log–log fitting method by using the Maximum Likelihood estimation (MLE). This method avoids binning of the data and construction of a histogram and, therefore, should be superior to the heuristic approach [37, 38]. Assuming that the power law holds for all observed values x_i, $i = 1, ..., n$ of x for which $x \geqslant x_{min}$, the analytical formula

$$\hat{\varepsilon}(v^2_{min}) = 1 + n\left[\sum_{i=1}^{n} \ln \frac{v_i^2}{v^2_{min}}\right]^{-1} \quad (1)$$

which yields the ML estimate $\hat{\varepsilon}$ for the exponent ε with a standard uncertainty of [37]

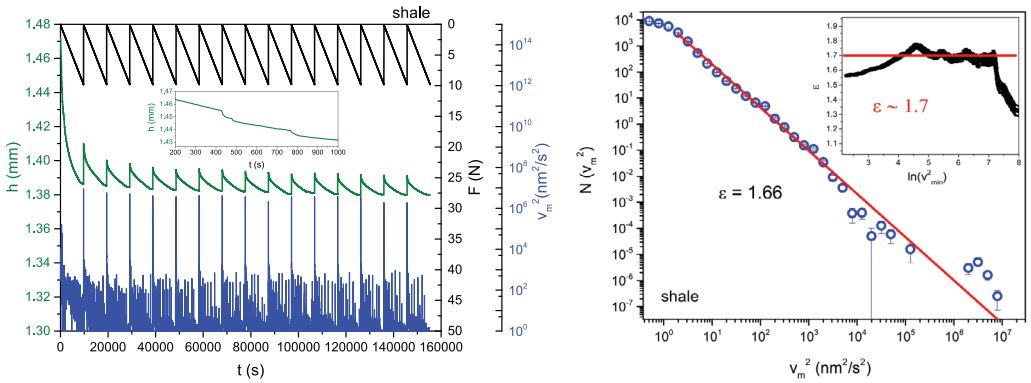

Figure 4. Left: compression experiment of shale at room temperature with several stress cycles. The green line displays the measured sample height h(t). The applied force is increased at the rate 120 mN min^{-1} from 0.01–10 N. Blue lines show the squared drop velocity maxima $v_m^2 = (\mathrm{d}h/\mathrm{d}t)^2_{\max}$. Right: corresponding log–log plot of the distribution N(v_m^2). The red line displays a power law with exponent $\varepsilon = 1.66 \pm 0.03$. The inset shows the corresponding maximum likelihood plot revealing a plateau at an exponent value of about $\hat{\varepsilon} = 1.70 \pm 0.05$

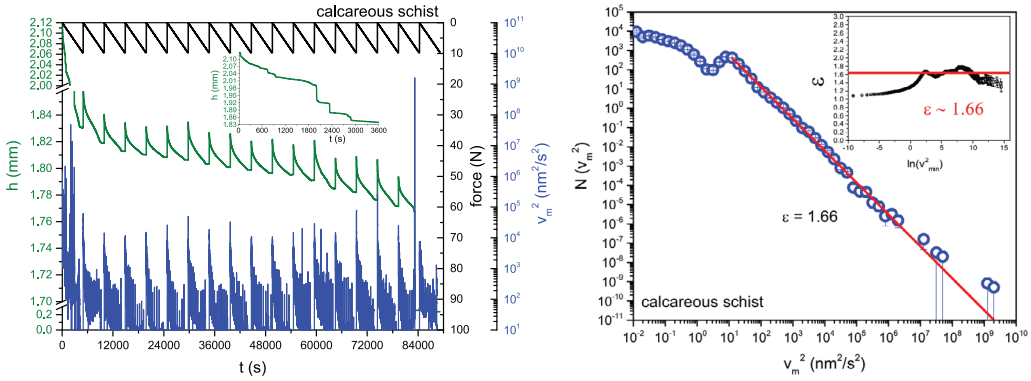

Figure 5. Left: compression experiment of calcareous schist at room temperature with several stress cycles. The green line displays the measured sample height h(t). The applied force is increased at the rate 120 mN min^{-1} from 0.01–10 N. Blue lines show the squared drop velocity maxima $v_m^2 = (\mathrm{d}h/\mathrm{d}t)^2_{\max}$. corresponding log–log plot of the distribution N(v_m^2). The red line corresponds to a power law with exponent $\varepsilon = 1.66 \pm 0.03$. The inset shows the corresponding maximum likelihood plot revealing a plateau at an exponent value of about $\hat{\varepsilon} = 1.66 \pm 0.12$

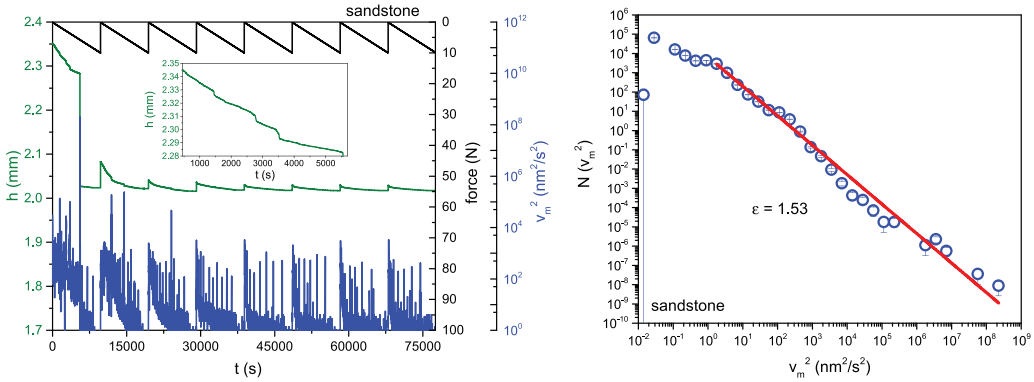

Figure 6. Left: compression experiment of sandstone at room temperature with several stress cycles. The green line displays the measured sample height h(t). The applied force is increased at the rate 60 mN min^{-1} from 0.01–10 N. Blue lines show the squared drop velocity maxima $v_m^2 = (\mathrm{d}h/\mathrm{d}t)^2_{\max}$. Corresponding log–log plot of the distribution N(v_m^2). The red line shows a power law with exponent $\varepsilon = 1.53 \pm 0.05$.

$$\sigma = \frac{\hat{\varepsilon}(v^2_{\min}) - 1}{\sqrt{n}} \tag{2}$$

represents the optimal guess based on the given data, with no need to perform any kind of fitting procedure. The plot of $\hat{\varepsilon}(v^2_{\min})$ should reveal a plateau at the most probable value of the exponent ε. However, it turned out that the MLE is biased unless n is large enough and even at n $\approx$ 200 systematic wavy oscillations are still observerd [3]. Unfortunately, the experimental data set consists only of a relatively small number of the biggest values that can be expected to contribute to the power law of the distribution. These oscillations may mask the

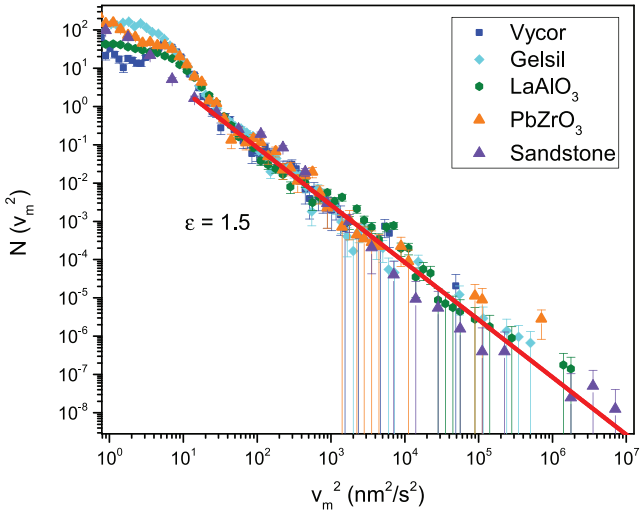

Figure 7. Log–log plot of the distribution $N(v_m^2)$ of maximum drop velocities squared of porous materials and ferroelastics. Both types of materials show similar power law behaviour yielding similar exponent values of $\varepsilon = 1.5$.

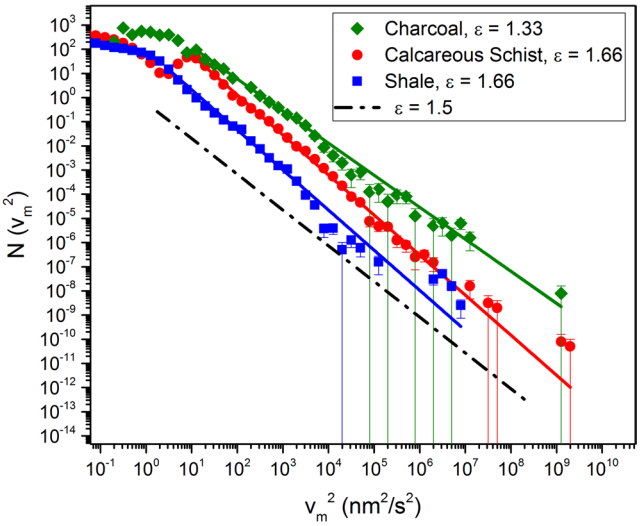

Figure 8. Log–log plot of the distribution $N(v_m^2)$ of maximum drop velocities squared of different rocks. The linear fits to the power laws of calcareous schist and shale reveal slightly higher exponents than to the fits of charcoal and sandstone. Curves have been shifted vertically for clarity, except for charcoal.

flat plateau naively expected in a MLE plot of an estimate of ε. Nevertheless, MLEs were performed for all measurements and the estimated exponents correspond to the approximately constant plateaus. The error of $\hat{\varepsilon}$ arises from the oscillations of the plateau region. MLE estimated and power law fitted exponent values are shown in table 3. For most experiments the exponent values from power law fitting and MLE are in good agreement within the error limits.

Figure 3 is an example of a distribution $N(v_m^2)$ of maximum drop velocities for the case of charcoal. The histogram displays the accumulation of signals over a single stress cycle. A plot of the MLE for $\hat{\varepsilon}(v_{\min}^2)$ is shown as inset. The power law exponent ($\varepsilon = 1.33 \pm 0.03$) agrees very well with recent studies, i.e. ($\varepsilon_{AE} = 1.32$) [39] and ($\varepsilon_{AE} = 1.3$) [40]. Figure 4 shows a stress cycle experiment of shale together with the corresponding log–log plot of $N(v_m^2)$ and the MLE diagram (inset). The exponent $\varepsilon \approx 1.7$ agrees quite well with [34].

As figures 4 and 5 show, shale and calcareous schist display similar power law exponents.

Figure 6 shows a compression cycle experiment of Yellow Sandstone, yielding $\varepsilon = 1.53$ in very good agreement with ($\varepsilon_{AE} = 1.49 \pm 0.05$) [2].

The ferroelastic materials ($LaAlO_3$, $PbZrO_3$) and the porous materials (Vycor, Gelsil, Sandstone), figure 7, reveal a similar power law behaviour and a linear fit with $\varepsilon = 1.5$ is a good estimate of all four velocity squared distributions $N(v_m^2)$. For comparison, calcareous schist and shale exhibit significantly higher values ($\varepsilon \simeq 1.7$), whereas for charcoal a lower value ($\varepsilon \simeq 1.3$) was found (figure 8).

5. Conclusions

In this paper we have reported the results of force driven compression experiments of several porous materials (Vycor, Gelsil, sandstone, shale, calcareous schist and charcoal) as well as some crystals ($LaAlO_3$, $PbZrO_3$) containing ferroelastic domain walls.

On a microscopic level the formation of avalanches in porous materials is quite different from domain wall systems, making a detailed comparison rather desirable. In porous materials avalanches appear as kind of chain reactions of collapsing pores in response to the applied compressive stress, whereas in domain wall systems a competition between random pinning and domain wall elasticity leads to the jerky response [42]. In addition domain walls are very 'lively' objects due to the fact that temperature can influence their behaviour drastically [43, 44].

The avalanche statistics for all the present systems was studied by measurements of the corresponding strain drops. From these strain drop data the corresponding peak velocities v_m where calculated and used to determine energy distributions $N(E \equiv v_m^2)$. These distributions yield power law behaviour $N(v_m^2) \propto (v_m^2)^{-\varepsilon}$, which in some favourable cases span over 6 orders of magnitude. Fitting the distributions and performing the corresponding MLEs we obtained with good accuracy $\varepsilon = 1.5$ (table 3) for domain walls, Vycor, Gelsil and sandstone, which agrees quite well with the mean-field result [15]. Our results seem to demonstrate the statement [15] of the maximum velocity distribution $N(v_m)$ to be a very robust experimental observable, even in the case of poor time resolution where the true maximum might v_m be missed, and a random velocity is picked out from each avalanche. In agreement with this, the maxima taken from our low-resolution time series, yield an inverse-squared power-law distribution $N(v_m) \propto (v_m)^{-2}$ for the above mentioned cases[5]. It should also be mentioned that although the time resolution (1 s) of our DMA apparatus is rather low, the driving rates are extremely small. To illustrate this with an example, the lowest force rate

[5] $\varepsilon = 1.5$ automatically implies for the velocity exponent $\mu = 2$.

(3 mN min^{-1}) used in our experiments corresponds to the addition of one A4-paper every 60 s.

Although many of the presently obtained exponents from strain drop data are rather close to the ones determined by AE, one should not push this similarity too far. One difference—despite the very different time resolutions—is given by the fact that AE measures integrated (over avalanche duration) energies, whereas—as already mentioned above—in our strain drop data we determine maximum velocities, from which we calculate maximum elastic energy releases $E_m \propto (v_m)^2$. Recently it was shown [41] that there exists a positive correlation between acoustic emission and force drops in strain driven compression experiments, although with some differences in the corresponding power law distributions. Our present results show that these correlations also exist for strain drops in stress driven experiments: by comparison of the exponents from strain drop data and AE (table 3) we find the same tendencies, i.e. similar exponents for Vycor, Gelsil and sandstone and a smaller one for charcoal and much larger values for shale.

Acknowledgments

The present work was supported by the Austrian Science Fund (FWF) Grant No. P28672-N36. AT acknowledges support from FWF Grant No. P27738-N28, and EV acknowledges support from the Spanish Ministry of Economy and Competitiveness (Project Nos. MAT2016-75823-R (AEI/FEDER, UE) and MAT2015-69777-REDT).

References

[1] Baró J, Corral Á, Illa X, Planes A, Salje E K H, Schranz W, Soto-Parra D E and Vives E 2013 *Phys. Rev. Lett.* **110** 088702
[2] Nataf G F, Castillo-Villa P O, Baró J, Illa X, Vives E, Planes A 2014 *Phys. Rev.* B **90** 022405
[3] Soprunyuk V, Schranz W, Tröster A, Puchberger S, Vives E and Salje E K H 2016 *Avalanches in Functional Materials and Geophysics, Understanding Complex Systems* ed E K H Salje *et al* (Berlin: Springer) (https://doi.org/10.1007/978-3-319-45612-6_4)
[4] Dimiduk D M, Woodward C, LeSar R and Uchic M D 2006 *Science* **26** 1188
[5] Miguel M-C, Vespignani A, Zapperi S, Weiss J and Grasso J-R 2001 *Nature* **410** 667
[6] Vinogradov A and Yasnikov I S 2014 *Acta Mater.* **70** 8
[7] Mäkinen T, Miksic A, Ovaska M and Alava M J 2016 *Phys. Rev. Lett.* **115** 055501
[8] Durin G and Zapperi S 2006 *The Science of Hysteresis* vol II, ed G Bertotti and I Mayergoyz (Amsterdam: Elsevier) pp 181–267
[9] Colaiori F 2008 *Adv. Phys.* **57** 287
[10] Barkhausen H 1919 *Phys. Z.* **20** 401
[11] Sethna J R, Dahmen K A and Myers C R 2001 *Nature* **410** 242
[12] Salje E K H and Dahmen K A 2014 *Annu. Rev. Condens. Matter Phys.* **5** 233
[13] Uhl J T, Pathak S and Schorlemmer D *et al* 2015 *Sci. Rep.* **5** 16493
[14] LeBlanc M, Angheluta L, Dahmen K and Goldenfeld N 2012 *Phys. Rev. Lett.* **109** 105702
[15] LeBlanc M, Angheluta L, Dahmen K and Goldenfeld N 2013 *Phys. Rev.* E **87** 022126
[16] Harrison R J and Salje E K H 2010 *Appl. Phys. Lett.* **97** 021907
[17] Harrison R J and Salje E K H 2011 *Appl. Phys. Lett.* **99** 151915
[18] Salje E K H, Zhang H, Idrissi H, Schryvers D, Carpenter M A, Moya X and Planes A 2009 *Phys. Rev.* B **80** 134114
[19] Carrillo L, Mañosa L, Ortín J, Planes A and Vives E 1998 *Phys. Rev. Lett.* **81** 1889
[20] Nataf G, Castillo-Villa P O, Sellappan P, Kriven W M, Vives E, Planes A and Salje E K H 2014 *J. Phys.: Condens. Matter* **26** 275401
[21] Castillo-Villa P O, Baró J, Planes A, Salje E K H, Sellappan P, Kriven W M and Vives E 2013 *J. Phys.: Condens. Matter* **25** 292202
[22] Bueble S, Knorr K, Brecht E and Schmahl W 1998 *Surf. Sci.* **400** 345
[23] Roberts S 1950 *J. Am. Ceram. Soc.* **33** 63
[24] Lines M E and Glass A M 1977 *Principles and Applications of Ferroelectrics* (New York: Oxford University Press)
[25] Glazer A M, Roleder K and Dec J 1993 *Acta Cryst.* B **49** 846
[26] Harrison R J, Redfern S A T and Salje E K H 2004 *Phys. Rev.* B **69** 144101
[27] Puchberger S, Soprunyuk V, Majchrowski A, Roleder K and Schranz W 2016 *Phys. Rev.* B **94** 214101
[28] Tanaka M, Saito R and Tsuzuki K 1982 *Japan. J. Appl. Phys.* **91** 291
[29] Chrosch J and Salje E K H 1999 *J. Appl. Phys.* **85** 722
[30] Levitz P, Ehret G, Sinha S K and Drake J M 1991 *J. Chem. Phys.* **95** 6151
[31] Eschricht N, Hoinkis E, Mdler F and Schubert-Bischoff P 2002 *Characterization of Porous Solids VI: Proc. 6th Int. Symp. on the Characterization of Porous Solids (COPS-VI) (Allicante, Spain, 8-11 May 2002) (Studies in Surface Science and Catalysis)* vol 144, ed F Rodríguez-Reinoso, p 355
[32] Eschricht N, Hoinkis E, Mädler F, Schubert-Bischoff P and Röhl-Kuhn B 2005 *J. Colloid Interface Sci.* **291** 201
[33] Blatt H and Tracy R J 1995 *Petrology: Ingneous, Sedimentary and Metamorphic* 2nd edn (New York: Freeman)
[34] Baró J, Planes A, Salje E K H and Vives E 2016 *Phil. Mag.* **96** 3686
[35] Ghaffar A 2014 Confinement induces structural changes of alkali metals in nanoporous system *PhD Thesis* University of Vienna
[36] Koppensteiner J 2009 The glass transition in nanoscale confinment probed by dynamic mechanical spectroscopy *PhD Thesis* University of Vienna
[37] Clauset A, Shalizi C R and Newman M E J 2009 *SIAM Rev.* **51** 661
[38] Deluca A and Corral A 2013 *Acta Geophys.* **61** 1351
[39] Jiang X, Jiang D, Chen J and Salje E K H 2016 *Am. Mineral.* **101** 2751
[40] Ribeiro H V, Costa L S, Alves L G A, Santoro P A, Picoli S, Lenzi E K and Mendes R S 2015 *Phys. Rev. Lett.* **115** 025503
[41] Navas-Portella V, Corral Á and Vives E 2016 *Phys. Rev.* E **94** 033005
[42] Paruch P and Guyonnet J 2013 *C. R. Phys.* **14** 667
[43] Salje E K H, Ding X, Zhao Z, Lookman T and Saxena A 2011 *Phys. Rev.* B **83** 104109
[44] Ding X, Lookman T, Zhao Z, Saxena A, Sun J and Salje E K H 2013 *Phys. Rev.* B **87** 094109